J. Neural Eng. **7** (2010) 045002 (12pp) doi:10.1088/1741-2560/7/4/045002

Acousto-optic laser scanning for multi-site photo-stimulation of single neurons *in vitro*

Bradley E Losavio[1], Vijay Iyer[2], Saumil Patel[3] and Peter Saggau[1]

[1] Baylor College of Medicine, Houston, TX, USA
[2] Howard Hughes Medical Institute, Ashburn, VA, USA
[3] University of Texas Medical School at Houston, TX, USA

Received 10 December 2009
Accepted for publication 12 April 2010
Published 19 July 2010
Online at stacks.iop.org/JNE/7/045002

Abstract

To study the complex synaptic interactions underpinning dendritic information processing in single neurons, experimenters require methods to mimic presynaptic neurotransmitter release at multiple sites with no physiological damage. We show that laser scanning systems built around large-aperture acousto-optic deflectors and high numerical aperture objective lenses provide the sub-millisecond, sub-micron precision necessary to achieve physiological, exogenous synaptic stimulation. Our laser scanning systems can produce the sophisticated spatio-temporal patterns of synaptic input that are necessary to investigate single-neuron dendritic physiology.

(Some figures in this article are in colour only in the electronic version)

1. Introduction

One of primary functional purposes of dendrites is to receive a multi-synaptic input, perform some modification to that signal and to transmit an output to other neurons. The various permutations of 'dendritic processing', 'biological computation' and 'dendritic physiology' are roughly synonymous to mean the handling of synaptic inputs for serving a role in the operation of the nervous system [1–3]. Specifically, the interactions among the thousands of synaptic inputs, often called *synaptic integration* or *synaptic summation*, comprise the computation [4–6]. These nonlinear synaptic interactions [7] can provide sophisticated input/output relationships [8], such as allowing neurons to behave as if they were a two-layer neural network [9–11]. Nonlinear synaptic summation would be notable because, theoretically, more powerful computational elements can be constructed from nonlinear subunits when compared to their linear alternatives. Implementing nonlinear functions, such as logarithms, polynomials and sigmoids, in dendritic hardware could therefore significantly expand the computational importance of single neurons.

The physiology of dendrites and synapses therefore merits a careful study. The interactions between synaptic inputs are due at least in part to the nonlinear, or 'active', properties of dendrites [12]. Synaptic inputs can engage voltage-gated ion channels [13, 14] as well as be reciprocally modulated by nonlinear ion channels [15, 16]. Furthermore, relatively constant, low-level synaptic activity influences the interactions between strong inputs [17]. All these interactions are augmented by the fact that the strengths of synapses themselves are dynamically modulated, in a process called 'synaptic plasticity' [18].

Single-neuron information processing is often studied by investigating the nature of synaptic summation. Various simulation [19] and experimental techniques have been used to investigate temporal integration [20], spatial integration [21–23], as well as the interactions between excitatory and inhibitory inputs [24]. Furthermore, investigations are ongoing into more complex facets of synaptic summation, such as the generation of dendritic action potentials [25, 26] and the storage of synaptic input patterns [27]. The potential of these more sophisticated functions highlights the importance of single-neuron computation in higher levels of behavior, both because it can serve a critical role in complex behavior that is attributable to a single neuron [28] and because functions previously thought to require a network of neurons may be possible at a single-neuron level [29].

Another reason for studying nonlinear synaptic interactions is that such a study might suggest the purpose of neurons' branched morphologies. Considering that a dendritic *structure* substantially dictates dendritic *function* [30, 31] and the fact that the synapses are spatially distributed across the exquisitely branched dendrites [32–34], it is reasonable to surmise that the dendritic structure would strongly influence synaptic summation. Indeed, previous studies have found that the dendritic structure regulates firing patterns (i.e. the output) [35], coincidence detection of multiple inputs [36] and propagation of action potentials [37]. The nonlinear synaptic interactions created by the dendritic branching patterns could thus provide a substrate for neural computation.

Given the strong linkage between neural information processing, dendritic physiology and nonlinear synaptic integration, it is paramount to develop experimental techniques for providing realistic, sophisticated patterns of synaptic activation. Multi-site photolysis of caged neurotransmitters provides this capability for two important experimental preparations: cultures of dissociated neurons and acute brain slices. The flexible multi-site photolysis necessary to do this is conveniently provided by fast laser scanning with acousto-optic deflectors (AODs). In this paper, we discuss the merits of multi-site neurotransmitter uncaging relative to other techniques for stimulating neurons and we provide arguments for using AODs for fast laser beam steering.

2. Why use caged neurotransmitters?

Several techniques have been used to excite single neurons. First, a neuron can be directly stimulated with an electrode. However, unless one uses extremely fine and closely spaced electrode tips, the stimulation is not focally restricted because the electric currents permeate over a region that might encompass several putative synapses. Furthermore, the mechanism by which this method excites the neuron is not precise: the experimenter cannot usually dictate whether the excitation is a result of stimulating neurotransmitter release from presynaptic terminals and/or recruitment of voltage-gated ion channels on the postsynaptic membrane. Additionally, direct electrical stimulation requires a high-precision manipulator for each stimulation electrode, practically limiting the experimenter to a few simultaneous sites. Finally, in acute brain slices, each insertion of an electrode damages the surrounding tissue.

Synaptic stimulation provides several advantages over direct electrical stimulation. Primarily, the experimenter utilizes the neuron's natural excitation mechanisms. The stimuli are thus likely to be more physiological and better replicate endogenous excitation. Two such techniques involve the rapid application of neurotransmitter by either iontophoresis or pressure ejection [21, 22, 38, 39]. However, these methods suffer from some of the same shortcomings as those of direct electrical stimulation: small numbers of invasive pipettes with inflexible positioning. Photolysis of caged neurotransmitters—an alternative method of synaptic stimulation—is not restricted in these ways [40]. Cleavage of the photolabile covalent bonds in the inert 'caged' molecules delivers neurotransmitters (e.g. glutamate) that are molecularly identical to those released by the presynaptic terminal [41]. With a properly focused light source, the bolus of the neurotransmitter that is created can be on the order of a femtoliter [42]. The synaptic activation pattern is restricted only by the positioning of the focus spots (section 4). Furthermore, the photolysis reaction is fast on a neurophysiological time scale, typically on the order of μs [43–45]. Whereas typical iontophoresis and pressure application distribute glutamate with a spatio-temporal resolution of 5–10 μm and 0.5–1 ms, caged glutamate photolysis offers much more focalized delivery of <1 μm and <1 μs. This improved resolution is critical for generating sophisticated patterns of synaptic activation as opposed to unspecific, bulk neural excitation. Finally, uncaging in acute brain slices has the additional advantage that the normal synaptic clearance mechanisms should cause the temporal concentration profile to closely mimic the natural synaptic kinetics.

3. Why use lasers for photo-stimulation?

Breaking the photolabile bond connecting the caging group and the parent molecule requires absorption of $>5.2 \times 10^{-19}$ J, equivalent to a single relatively energetic photon with a wavelength of $\lambda < 380$ nm (i.e. ultraviolet (UV) range [46]). Arc lamps [47], flash lamps [48] and high-intensity light-emitting diodes [49] can serve this purpose, but lasers are often more convenient. Since they are monochromatic, all of a laser's intensity is concentrated into the useful wavelengths whereas large portions of a lamp's emission spectrum may have to be discarded by filtering. Furthermore, it is often easier to select dichroic mirrors, in addition to obviating the bandpass filter, by using a single wavelength. Most importantly, since the laser output is collimated, it is much easier to focus on a diffraction-limited spot in comparison with the natural angular divergence of a lamp.

Since single-photon photolysis is performed in the UV regime, it is most intuitive to incorporate a laser that produces light in that wavelength range. In fact, this choice would be satisfactory for optically thin neuron specimens (section 5). However, a pair of photons—each with half the requisite photolysis energy, corresponding to wavelengths of $\sim$700 nm—could instead break the photolabile bond. Two-photon photolysis with near-infrared (NIR) light from an ultrafast pulsed laser outperforms one-photon UV photolysis in light-scattering neuron preparations (section 6). NIR wavelengths are much less sensitive to Rayleigh scattering than UV and can therefore penetrate a few hundred microns into scattering tissue with high resolution [50, 51]. Furthermore, because of the intrinsic optical sectioning of multiphoton absorption, the axial resolution is vastly superior [52–55]. After carefully considering their various merits, selecting the most suitable laser components for a particular experimental goal (section 7) extracts the most advantages from photolytic stimulation.

4. Why use acousto-optic deflectors for laser beam steering?

To fully realize the advantages of photolytic stimulation, one must choose how to optimally direct the laser beam to the specimen. Optical fibers offer several compelling features [56]. First, the laser can be placed relatively distant from the microscope setup, adding flexibility to the laboratory layout. Second, the laser beam can be split and coupled into multiple fibers, allowing multiple stimulation sites with only a single laser. Third, a single, high-power laser can be shared between multiple microscope setups. Finally, with appropriately tapered fibers, photolysis laser light can provide relatively high spatial resolution (i.e. $<5\,\mu$m [20]). While ultrafast pulsed NIR laser light provides significant benefits in resolution, one disadvantage to using optical fibers in this application is that they add a large amount of group velocity dispersion (section 6, [51, 55, 57]). This issue can be addressed by using photonic crystal fibers specially designed to add no dispersion at one particular wavelength, but the fundamental limitation remains: each photolysis site requires one fiber and each fiber requires a manipulator. Optical fiber delivery thus has little advantage over pipette-based stimulation techniques.

Instead of positioning the laser beam by physically moving the transmitting fiber, one should steer the laser beam as rapidly as possible. This steering can be accomplished by reflective or diffractive optics [58]. The large majority of commercially available laser scanning microscopes are constructed by attaching a pair of mirrors to two orthogonal galvanometers. The scan speed is limited, however, by the inertia of physically moving mirrors: most microscopes are limited to a few hundred hertz in line-scanning mode and are unable to perform fast arbitrary jumps across the field of view (FOV). Since neurons do not typically grow conveniently along straight lines, galvanometer-based laser scanning systems are ill-suited for multi-site photolysis systems.

Diffractive optics—such as liquid crystals on silicon (LCoS) and AODs—offer rapid, inertia-free laser beam steering [57, 59–64]. The limitation of scanning speed for a diffractive element is the speed at which it can change its virtual grating constant, typically less than a millisecond. In contrast to galvanometer laser steering, there is no time penalty levied for a jump across the FOV relative to a jump between neighboring points. We chose AODs for fast, inertia-free laser beam steering because they offer diffraction-limited spatial resolution, μs temporal resolution, intrinsic laser intensity modulation, high damage threshold for continuous and pulsed lasers and the possibility of combining scanning with spectral and temporal dispersion compensation for ultrafast laser pulses [65, 66].

The basic purpose of an AOD is to rapidly change the direction of the laser beam [67, 68]. A radio frequency (RF) sound wave in an acousto-optical medium establishes a virtual diffraction grating, which produces the desired beam deflection. Because the frequency of the RF wave is rapidly tunable, the change of the deflection angle is likewise fast. The sole limitation of scanning speed is thus the time required for the sound wave to fill the optical aperture, i.e. the physical size of aperture divided by the speed of sound in that medium. This aperture time is typically on the order of a few microseconds, much faster than typical inertia-limited galvanometer-based scanning instruments.

Like all laser scanning systems, the angular deflections imparted by the AODs are not immediately useful: the angle changes must be converted to position changes in the specimen plane. A lens (i.e. the objective lens) performs a Fourier transform between its focal planes, converting different angles at the back focal plane to corresponding positions in the image plane (figure 1). In a similar manner, lenses serve another critical role in the practical construction of an AOD-based scanning system. They provide a means to effectively relay the angle changes created by the AODs to the objective lens' back focal aperture (BFA) without obstructions (figure 2). Even though these deflection angles are small (on the order of tens of mrad), after the propagation of >1 m, the scan pattern is too large to be accommodated by the various apertures of the optical path. We thus use pairs of lenses arranged in a $4f$ configuration (a 'telescope') to relay the principal optical planes (figures 1 and 2). In this manner, all the diffraction planes remain confocal with one another while the angular spread of the scan pattern is easily encompassed by standard diameter lenses. In our configurations, we insert full beam aligners (i.e. an orthogonal mirror pair) between the AODs and relay telescopes so that scan patterns can propagate through the centers of the lenses (figure 2).

Our two basic AOD scanning schemes are illustrated in figure 1. The simpler of the two involves a pair of orthogonal AODs with circular apertures (figure 1(a) and section 6). The circular aperture permits the use of a collimated laser beam that has been expanded to match the aperture's diameter. Since the AOD's angular resolution directly influences both the imaging and photolysis resolution, exactly filling the AOD aperture ensures that we obtain the AOD's full resolution because diffraction at an aperture is inversely proportional to the aperture diameter. A telescope formed from two spherical lenses relays the diffraction plane of the vertically deflecting AOD to the horizontally deflecting AOD. A series of successive telescopes relay the resulting image plane to the specimen plane of the objective lens. Using AODs with elongated apertures (section 5) requires modifications to this scheme (figure 1(b)). Four cylindrical lenses, a pair forming an anamorphic telescope for each AOD (figure 2), compress the expanded laser along the narrow axis of the aperture. Since the AODs deflect along the long axis, this has a negligible effect on the deflection. The full angular resolution is available with minimal intensity losses.

5. Ultraviolet photo-stimulation of cultured neurons

An AOD-scanned UV laser beam can provide physiological multi-synaptic activation to sparse, dissociated neuron cultures. Such a system can activate tens of synapses quasi-simultaneously by creating sophisticated spatio-temporal distributions of the neurotransmitter [69, 70].

The system we built is based upon a diode-pumped, solid-state, frequency-tripled Nd:YVO_4 laser (DPSS model #3505).

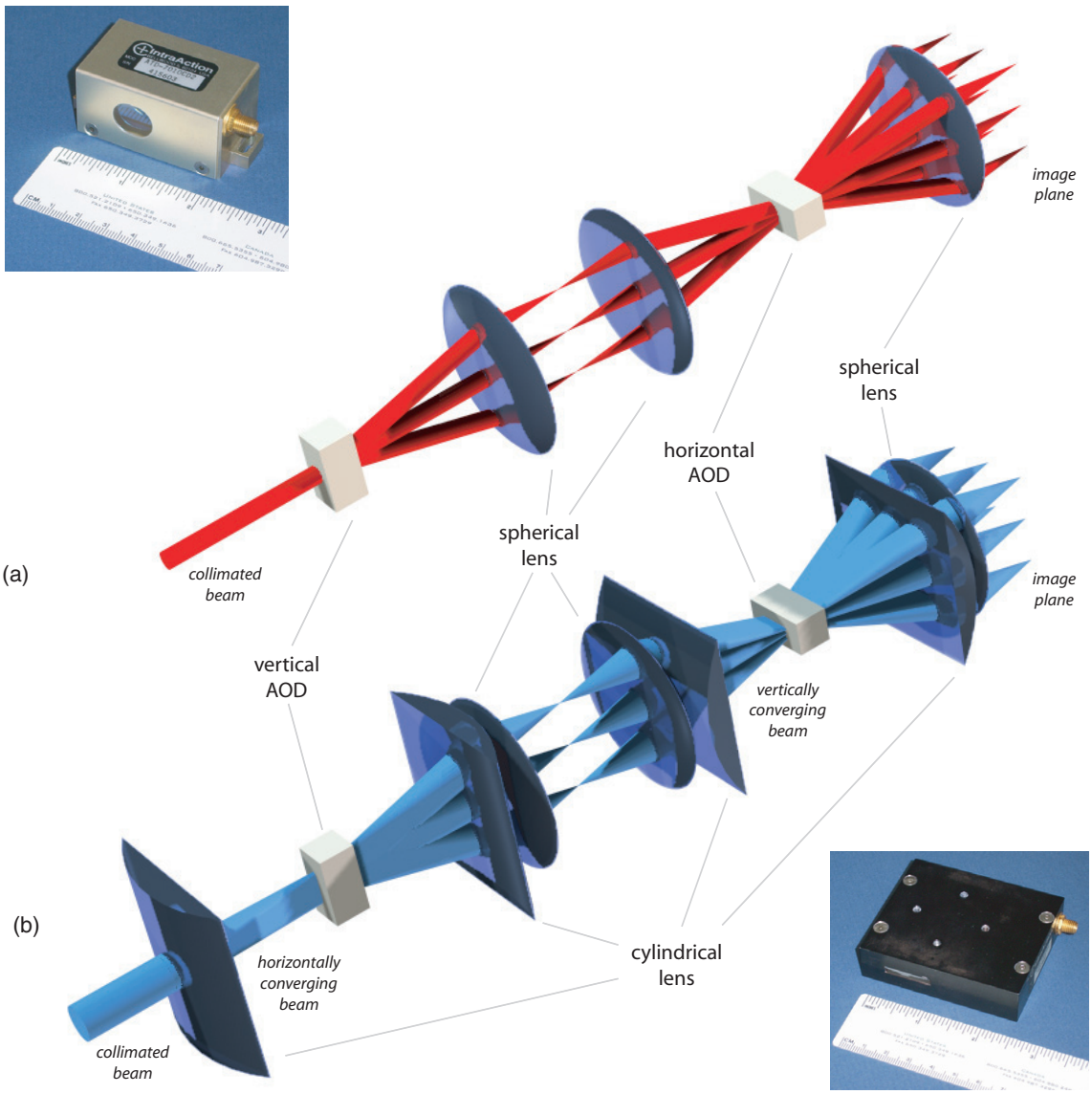

Figure 1. Principles of AOD scanning. (a) Scheme using circular aperture AODs. To make use of the AODs' full resolution, a collimated laser beam exactly fills the circular aperture (inset). The first AOD imparts a vertical angle change to the beam. A 1:1 telescope, consisting of two spherical lenses, relays this diffraction plane to the second AOD, which confers an angle change in the horizontal dimension. A final imaging lens converts the angle into a focused point displaced from the optical axis. Lateral displacements in the specimen plane result directly from different entry angles into the objective lens back focal aperture, several relay telescopes downstream (figure 2). While the figure depicts several spots being simultaneously scanned, in practice the AODs rapidly scan among the desired angles, limited only by the time required for the acoustic wave to fill the aperture, creating a 'quasi-simultaneous' multi-site pattern. (b) Scheme using elongated aperture AODs. Again, to fully utilize the AOD's full resolution, the laser beam should fill the aperture, but in this case, the AOD's aperture is not circular, but rectangular (inset). We therefore modify the scheme in (a) by inserting a pair of cylindrical lenses to compress the beam in the non-scanned dimension ('converging' beams). This has no effect on the orthogonal dimension, which is deflected as before. Note: figure is not drawn to scale; distances and angles are exaggerated for clarity.

The output is pulsed at 50 kHz via an externally clocked Q-switch. The external-clocking allows us to synchronize the 20 ns pulses with the AOD scan patterns. With 1 W of output intensity at $\lambda = 355$ nm, the laser provides plenty of excess intensity to cope with loses along the optical path, such as the ~70% diffraction efficiency of each AOD. We inserted a multi-order quartz waveplate (CVI Laser QWPM-355-05-4-R10) to optimize the polarization for input to the AODs (figure 2(a)).

A pair of orthogonal, fused silica AODs (IntraAction SDM-1502B8, figure 1(b), inset) steer the UV laser in the two lateral dimensions. Because shorter wavelengths are diffracted to a lesser extent, deflecting UV wavelengths requires large effective apertures to realize suitable angular resolution. These deflectors have a 20 × 2 mm aperture, capable of producing $N = 384$ resolvable spots given a $\Delta f = 100$ MHz acoustic bandwidth and $v = 5917$ m s^{-1} speed of sound. Operating in the Bragg configuration, the scan angle subtends $\theta_{\text{scan}} = \lambda \Delta f / v = 5.99$ mrad. Two drivers (IntraAction DE-1503M), one per AOD, provide the 100–200 MHz RF input for the beam deflection. The drivers can also modulate the intensity

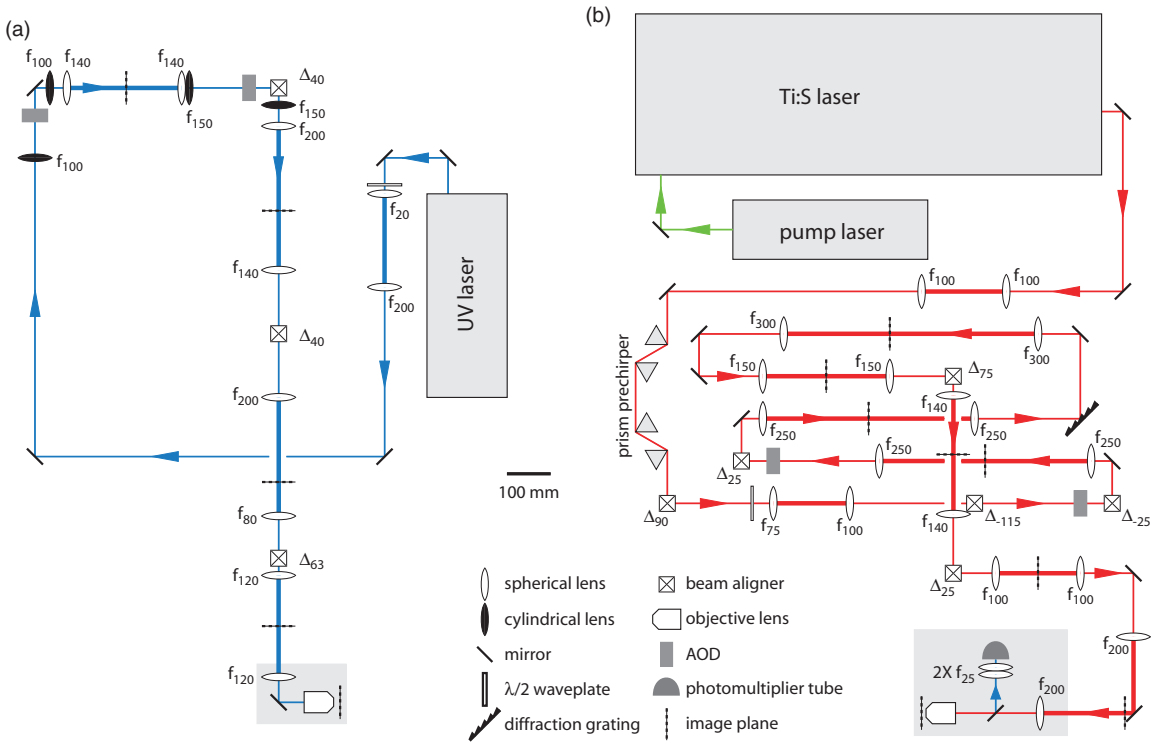

Figure 2. Optical layout of AOD scanners. Telescopes relay the scan pattern from the image planes (*dashed* lines) to the specimen plane of the microscope objective lens. A thickened laser beam indicates a lens pair that forms a telescope. (a) UV scanner. A pair of cylinder lens telescopes compresses the laser beam (blue) in the unscanned dimension. (b) NIR scanner. A diffraction grating and prism prechirper (prechirper not drawn to scale) compensate for spectral and temporal dispersion of ultrafast laser pulses (red). For more details, see [73]. Note: lens focal lengths (f_x) and beam aligner height changes (Δ_x) in mm.

of the deflected beam by scaling the 0–3 W acoustic power. We use this feature in two situations. First, the early pulses after the Q-switch has been activated are generally of much higher intensity; we attenuate these first few pulses until their intensity reaches a steady state. Second, we sometimes grade the intensity of each photolysis site on a point-to-point basis to normalize the synaptic activation.

The deflected UV laser beam is relayed to an inverted microscope (Zeiss Axiovert S100 TV) with fused silica lenses (Linos Photonics) and high-energy dielectric mirrors (Linos Photonics DLHS350). We evaluated several optical layouts for our UV laser scanner. We first investigated an all-spherical lens system that scanned a ∅2 mm laser beam, but the resulting 38 spot resolution was too coarse for focal photolysis. To increase the resolution by filling more of the AOD's elongated aperture, we explored anamorphic systems. Our second design, slightly modified from Xu and Stroud [68], improved the number of spots as expected, but the resolution was limited by astigmatism. Our final design incorporated a modification of our all-spherical lens system (figure 1(a)) wherein a cylindrical lens telescope is added for each AOD (figure 1(b)). We use a pair of fused silica cylinder lenses to focus and re-collimate the ∅20 mm in the unscanned dimension (figure 2(a)). Following the creation of the two-dimensional scan pattern (384 spots along each dimension), we employ a series of $4f$ telescopes to relay the scan pattern to the microscope. A pair of demagnifying telescopes (1.4× and 2.5×) reduce the ∅20 mm beam to slightly overfill the ∅5 mm objective lens BFA (figure 2(a)).

In the microscope, the scan angles are translated to a scan pattern with a high-magnification, high numerical aperture (NA) objective lens. For focusing in this application, a quartz objective lens specifically designed for UV light would seem ideal. Interestingly, in our experience, commercially available lenses that are specified for these short wavelengths (Zeiss *Ultrafluar*, for example) transmit UV light less efficiently than their standard counterparts. We observed more efficient UV transmission and smaller focal volumes (data not shown) with a water-immersion objective lens (Zeiss 63× *C-Apochromat*, 1.2 NA) compared to an oil-immersion objective lens (Zeiss 100× *Fluar*, 1.3 NA). We suspect that this superiority is a result of the better refractive index matching between the immersion medium and the embedding medium (i.e. saline perfusion solution).

For instrument control, we developed custom software written in C to run on a personal computer (PC). To synthesize the AOD control signals, we employed a pair of 12-bit, 2-channel arbitrary waveform function generators (Keithley PCIP-AWFG). The four D/A channels generated the frequency modulation (FM) and amplitude modulation (AM) signals (buffered to drive the 50 Ω AOD driver inputs, Analog Devices BUF04), while the synchronous digital channels gated the UV laser's Q-switching. A master clock at 100 kHz synchronized all the hardware (Innovative Integrations Chico). The custom software overlays the site-selection graphical user interface (GUI) with a bright-field image from a video camera (figure 3(a), *right*; Panasonic WV-1550 with 0.75–3× par-focal zoom lens, Edmund Scientific VZM 300) captured with

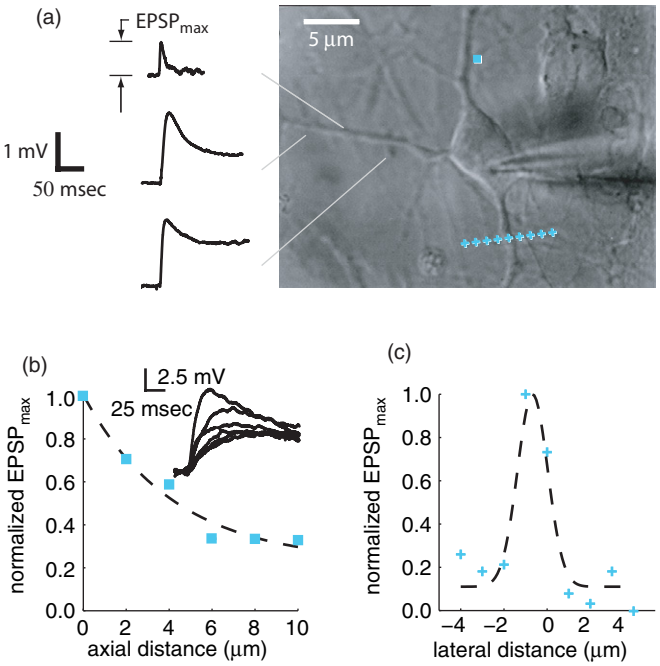

Figure 3. Demonstration of photolysis with the UV scanner. (a) Right: bright-field image of hippocampal neuron in low-density dissociated culture. *Square* and *plus* markers indicate photolysis sites of data in (b) and (c), respectively. Left: example voltage transients recorded by somatic current clamp in response to photolytic stimulation (5–10 pulses) at the indicated sites. (b) Axial resolution. $EPSP_{max}$ decreases as the objective lens was iteratively moved away from the initial focal plane. Inset: somatic EPSPs in response to optical stimulation at the position indicated by the *square* marker in (a). The dashed line indicates an exponential fitting with $1/e = 7.1\ \mu$m. (c) Lateral resolution. Nine photolysis sites were placed along a line perpendicular to the dendrite (*plus* markers in (a)). $EPSP_{max}$ in response to photolysis at each of these locations is plotted versus distance from the dendrite. The dashed line indicates a Gaussian fitting with a FWHM $= 2.34\ \mu$m and an offset $= -0.7\ \mu$m.

a frame-grabber (MuTech IV-400). Registration between the camera image and the UV scanner is accomplished by manually adjusting the limits of the FM signals in the custom software. The electrophysiology signals from a patch clamp amplifier (Dagan BVC-700A) were digitized with a 12-bit data acquisition card (Measurement Computing CIO-DAS08).

We judged low-density, dissociated neuron cultures to be particularly advantageous for this fast-scanning system. First, being only a single cell layer thick, their optical thinness decreases light-scattering. Second, because of their two dimensionality, all of a neuron's dendrites and soma lie in the same geometric plane. This eliminates the need for complex focusing mechanisms. Third, the sparse density renders simple the task of associating a neuron with its branches. Finally, since cultures are grown extensively in an incubator, we gain the ability to genetically or molecularly manipulate them. We utilized serum-free cultures [71] from embryonic (E19) Sprague Dawley rat hippocampus plated at 20 cells mm^{-2} onto glass-bottom Petri dishes (MatTek P35-G-1.5-14-C and P35-G-0-14-C) coated with poly-L-lysine (0.1 mg ml^{-1}, Sigma P-2636). Electrophysiology recordings were performed for 14–21 days *in vitro*.

Figure 3 illustrates typical responses of a cultured hippocampal neuron to UV photolytic stimulation controlled by AODs. A peristaltic pump (10 ml min^{-1}) continually perfused a solution containing (in mM) 135 NaCl (all chemicals from Sigma unless otherwise noted), 3 KCl, 1.25 Na_2HPO_4, 31 D-glucose, 10 HEPES, 2 $CaCl_2$ and 2 $MgSO_4$, pH adjusted to 7.3, with NaOH and 200 μM α/γ-bis-CNB-glutamate (Invitrogen, [72]) at 22 °C. We established current-clamp recordings from the neurons (figure 3(a), right) with pipettes containing (in mM) 152 Kgluconate, 10 HEPES, 2 $MgCl_2$, 2 MgATP, 0.3 NaATP and 1 BAPTA, pH adjusted to 7.3, with KOH. Steering the laser beam to a user-selected site for 5–10 pulses generated somatic voltage transients that somewhat mimic excitatory postsynaptic potentials (EPSPs; figure 3(a), left). Some transients exhibited fast decay to the baseline (*top* trace) while stimulation at other sites showed sustained depolarizations for many tens of milliseconds (*bottom* two traces). To demonstrate that we were indeed observing synaptic activation, we removed caged glutamate from the bath as well as placed photolysis sites >25 μm from the dendrite in the presence of caged glutamate. In both of these experimental controls, we never observed a distinguishable response (data not shown). Iteratively displacing the focal plane above that of the neuron while still stimulating the same *X*–*Y* location (figure 3(a), square marker on the *right* panel) resulted in diminishing $EPSP_{max}$ (figure 3(b)), defined as the peak EPSP amplitude (figure 3(a), *top* trace on the left). An exponential curve fit indicates that the $1/e$ axial resolution of photolysis for this system is 7.1 μm. (Throughout this paper, we fit data sets with the most subjectively obvious mathematical function. We do not intend to imply that any particular fitted function accurately models the underlying physical phenomenon.) To test the lateral resolution, we successively stimulated points perpendicular to the neuron's dendrite (figure 3(a), *plus* markers). From this test, we find that the lateral resolution is 2.3 μm, as indicated by the full-width half-maximum (FWHM) of a fitted Gaussian curve (figure 3(d)). The largest $EPSP_{max}$ is not observed for the site that directly overlays the dendrite, but is instead displaced 0.7 μm to one side. We conclude that this location optimally stimulates the neurotransmitter receptors as opposed to placing the photolysis directly on the dendrites.

6. Near-infrared photo-stimulation of acute brain slice neurons

To investigate synaptic interactions in light-scattering brain specimens, such as acute brain slices or organotypic brain slice cultures, we developed a multi-site scanning system that uses multiphoton photolysis. This system, constructed from an ultrafast pulsed laser and a pair of orthogonal circular aperture AODs (figure 1(a), inset), is detailed in another publication [73]. In brief, a collimated NIR laser beam is deflected by a vertical AOD, the diffraction plane is relayed to the horizontal AOD with a spherical lens telescope and the two-dimensional scan pattern is relayed to the objective lens by

another series of telescopes (figures 1(a) and 2(b)). Because of the wide spectral bandwidth of the ultrashort laser pulses, we were required to compensate for the significant spectral and temporal dispersions imparted by the AODs [74, 75]. To address the spectral dispersion, we inserted a diffraction grating to re-align the diverging spectral components [73]. To compensate for the temporal dispersion, we introduced a prism-based prechirper to pre-condition the pulses so that, at the specimen plane, the original pulse width was nearly restored [73, 76–78].

We tested our NIR photolysis system using neurons in acute brain slices. We obtained brain slices of rat hippocampus according to guidelines approved by the Institutional Animal Care and Use Committee at Baylor College of Medicine. Anesthetized Sprague Dawley rats were trans-cardially perfused with an ice-cold solution containing (in mM) 110 ChCl, 2.5 KCl, 1.25 Na_2HPO_4, 10 D-glucose, 25 $NaHCO_3$, 0.5 $CaCl_2$ and 7.5 $MgCl_2$. Brain slices (350 μm thick) were transferred to solution containing 125 NaCl, 2.5 KCl, 1.25 Na_2HPO_4, 10 D-glucose, 25 $NaHCO_3$, 2 $CaCl_2$ and 2 $MgCl_2$, 1.3 ascorbate, and 3 pyruvate for 20 min at 34 °C and then at room temperature for 40 min before the experiment.

This scanning setup is quite successful at precisely stimulating neurons in acute brain slices. However, to precisely place photolysis sites, the experimenter must be able to distinguish the neuron from its surroundings. Obtaining a high-resolution structure is more straightforward with the NIR scanner than with the UV scanner. Dialyzing a fluorescent dye through the patch pipette allows us to collect a high-contrast image ($\lambda_{excitation}$ = 720 nm) that clearly shows the dendritic spines (figure 4(a), ~7 mW laser power measured at the objective lens BFA). Lower laser power, shorter pixel dwell time (25 μs) and the absence of caged glutamate eliminate possible photolytic responses during imaging. Testing various dyes for strong fluorescence resulting from two-photon excitation at this wavelength, we found the strongest signal from the calcium indicator bis-FURA-2, which we used solely as a structural indicator. Neurons were patch-dialyzed with a 333 μM bis-FURA-2 (Invitrogen-Molecular Probes) fluorescent dye solution containing (in mM) 120 K-gluconate, 20 KCl, 10 HEPES, 2 $MgCl_2$, 0.2 EGTA, 4 Mg-ATP, 0.3 Tris-ATP and 7 phosphocreatine) for at least 15 min. The custom scanning software for this setup, written in Matlab (with the DAQ Toolbox, Mathworks), rasters the AODs across the objective lens FOV to generate a fluorescence image. A stepper motor connected to the objective lens fine focus knob allowed the software to construct a three-dimensional (3D) image volume. Figure 4(a) is a montage of maximum projections of six overlapping image volumes that contained a hippocampal CA1 pyramidal neuron. Zooming in to a smaller FOV illustrates that dendritic spines are clearly resolvable (insets in figures 4(b), (c) and (e)). From these zoom-ins, the experimenter can select photolysis sites at putative synapses (figure 4(b), inset).

After the initial dye-filling period, low positive pressure (~0.04 psi) was applied to a large-bore pipette filled with 12 mM MNI-glutamate (Tocris [79]). The ejected plume

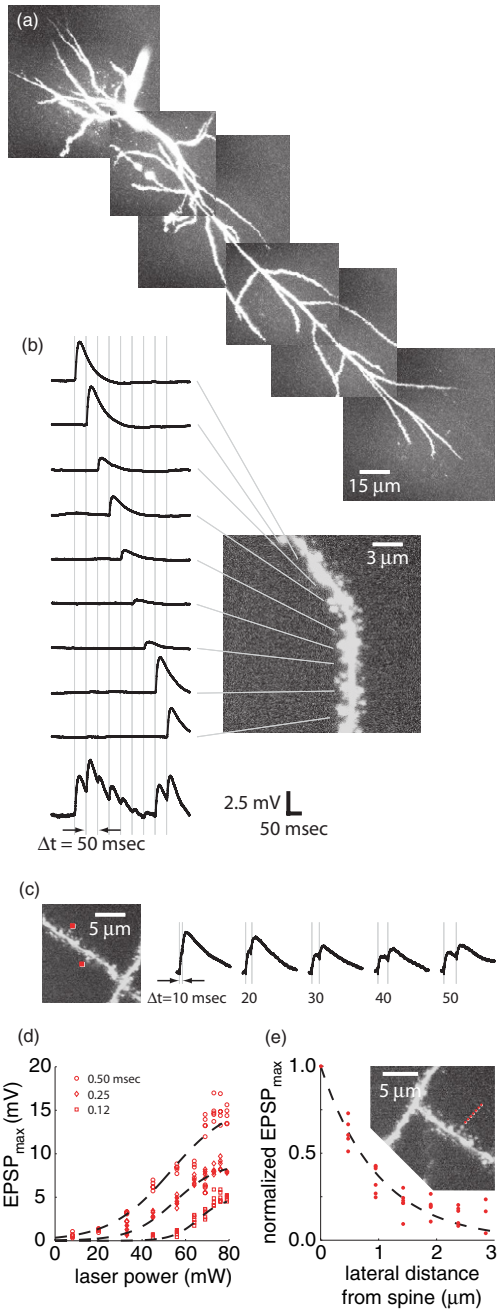

Figure 4. Demonstration of photolysis with the NIR multiphoton scanner. (a) Fluorescence montage composed of six maximum projections of a bis-FURA-2-filled CA1 hippocampal neuron in an acute brain slice. (b) Spatial summation. Nine sites were successively stimulated by multiphoton photolysis at the indicated spines. The traces illustrate the somatically recorded voltage transients in response to each individual stimulation. A tenth trace (*bottom*) shows the cellular response to all nine sites activated with a delay of Δt = 50 ms during the same recording. (c) Two-site temporal summation. Two neighboring spines (indicated by *square* markers) were stimulated with varying delays (Δt = 10–50 ms) (d) Grading photolysis strength with AOD modulation of laser intensity. Normalized EPSP amplitudes are plotted as a function of laser power for 0.12, 0.25 and 0.5 ms pulses. Dashed lines indicate sigmoid fittings. (e) Lateral resolution. Similar to figure 3(b), a series of photolysis arranged perpendicular to a spine head indicates the decrease in response as a function of distance from a putative synapse. The dashed line indicates an exponential fitting with $1/e = 0.99\,\mu$m.

of caged glutamate bathes the neuron over a region slightly larger than the objective lens FOV. A 0.1–0.5 ms duration laser pulse at 720 nm (∼21 mW) located just adjacent to a spine head results in a 0.5–3 mV amplitude EPSP measured at the soma (figure 4(b), *traces*). With an inter-site delay of $\Delta t = 50$ ms, the response to stimulating all nine sites is shown in the bottom trace. Comparing the individual responses to the combined response constitutes a basic spatial summation experiment. The $EPSP_{max}$ varies for each location because the photolysis location is not optimized to coincide with the neurotransmitter postsynaptic density 'hot spots' [80, 81] and each synapse could have a variable response to an identical application of neurotransmitter [18, 82]. We developed an automated software routine that optimizes the *X*–*Y* location of each photolysis site and then tunes the laser intensity at each site to obtain a particular desired $EPSP_{max}$. Figure 4(c) provides an example of tuned stimulation as well as a simple demonstration of a temporal summation experiment. A pair of spines are stimulated on successive sweeps wherein Δt ranges from 10 to 50 ms. The decline in $EPSP_{max}$ as Δt increases gives an indication of how sensitive the neuron is to coincident inputs.

We also characterized the effects of laser intensity modulation and resolution on the photolytic responses. Modulating the amplitude of the RF acoustic wave in the AOD allowed us to change the laser power on a site-to-site basis at the same speed as the laser was deflected. In general, increasing the laser power delivered to a particular photolysis site resulted in a larger $EPSP_{max}$ (figure 4(d)). Similarly, we could modulate the $EPSP_{max}$ by changing the dwell time (i.e. length of the photolysis pulse) at each site (0.12–0.5 ms). This highlights the fact that in this regime of laser power and dwell times, the total energy delivered dictates the neuron's response to a photolytic stimulation. A 0.5 ms, 45 mW pulse produces a similar $EPSP_{max}$ as a 0.25 ms, 75 mW pulse. For the spatio-temporal summation experiments we typically perform, we use 0.5 ms pulses of ∼20 mW to generate $EPSP_{max}$ on the order of a few mV. We chose these parameters because they allow us to use lower laser intensities while still providing acceptable temporal resolution to study the features in which we are interested. If higher temporal resolution and/or more quasi-simultaneous photolysis sites are needed, then the system is capable of shortening dwell times by increasing photolysis intensity. Similar to figure 3(c), we investigated the lateral photolysis resolution by placing photolysis sites along a line perpendicular to the dendrite and passing through a spine head (figure 4(e), inset). The normalized $EPSP_{max}$ decreases with increasing distance from the spine head, indicating that the spatial resolution in the focal plane is <1 μm (FWHM, figure 4(d)). In a previous paper, we demonstrated the axial resolution of this system to be <2.5 μm [73]. This combined 3D resolution is sufficient to optically stimulate individual spine heads. Placing the photolysis site >10 μm from a spine or not applying caged glutamate failed to elicit an observable response (data not shown), confirming that our instrument was synaptically evoking the EPSPs. Furthermore, photolysis while blocking glutamate receptors with 10 μM CNQX and 50 μM D-APV (both from Tocris) never resulted in any transients that could be distinguished from noise (data not shown), also suggesting that the EPSPs were generated by activating postsynaptic glutamate receptors.

7. Discussion

Photolytic stimulation with an AOD-scanned laser beam and caged neurotransmitters offers several compelling advantages over classical electrical stimulation techniques. Optical stimulation is more precise, less invasive and makes possible the flexible positioning of multiple stimulation sites. Furthermore, the optical stimulation more closely mimics endogenous synaptic release of the neurotransmitter when compared to electrical activation of voltage-gated ion channels.

There are a few limitations to consider, however. First, optical stimulation is restricted to either excitation or inhibition. Because of the large absorption spectrum of the available caging groups [46], it is not possible to discriminate between two caged compounds. Thus, presently one cannot optically release an excitatory caged neurotransmitter independently of an inhibitory caged neurotransmitter. This is a limitation shared by direct electrical stimulation, but not by iontophoresis (section 2). However, there remains a limitation on the number of stimulation pipettes that can be arranged around a typical neural specimen. Second, photolytic stimulation is restricted to the FOV of the microscope objective lens. A larger FOV from a lower magnification objective lens usually results in a compromise on imaging resolution, thus limiting the focality of stimulation. This might be mitigated by selecting one of the objective lenses that combine low magnification (∼20×) and high numerical aperture (∼1.0). Studying the nonlinear interactions between hundreds or thousands of synapses highlights a limitation of any stimulation system: accurately locating the multitude of stimuli. Even with a clear, high-contrast, high-resolution image, it would take a human experimenter many minutes to mark every suspected synapse (e.g. with a point-and-click device). One possible solution involves automated image processing to identify dendrites [83, 84] and putative synaptic sites [85, 86]. Such an approach is feasible within the GUI of our scanner software but is less straightforward to implement with pipette-based techniques.

Finally, photolytic stimulation is best suited to studying single neurons with *in vitro* preparations, as opposed to *in vivo* studies. First, the caged neurotransmitter must be continually applied, a task difficult to do outside of a specimen chamber. A recent alternative, single neurons expressing genetically encoded light-sensitive ion channels—for example, channelrhodopsin—might extend the ability of AOD-based multi-site scanning to investigate this facet of neurophysiology *in vivo* [87–91]. Somewhat implicit in our discussion, we have focused on applying photolytic stimulation techniques to studying the physiology of a single neuron. While these AOD scanners are fully capable of stimulating any neuron that is within its FOV, establishing somatic recordings from multiple neurons somewhat obviates the advantages of multi-site photolytic stimulation. On the other hand,

only such an instrument is capable of investigating the role of nonlinear synaptic interactions in networks of multiple neurons. Merely recording the voltages at a small handful of somata would require all of the available space around a typical preparation, leaving none for pipette-base stimulation. Interestingly, multi-site *optical* recording of membrane voltage or intra-cellular calcium concentration combined with multi-site optical stimulation might enable one to study these aspects of neurophysiology (see below).

Our AOD-based UV scanner (section 5) presents several interesting features for performing photolytic stimulation. UV lasers are generally simpler and cheaper than their ultrafast NIR counterparts. Furthermore, the ability to use cultured neurons is often convenient. Cultures can be prepared ahead of time to differing specifications (i.e. cell density, etc). During their long-term incubation, investigators can apply genetic manipulations to cultures, such as viral transfection, providing experimental possibilities that are not straightforwardly available with acute brain slices.

Our enthusiasm for AOD-based UV photolysis is tempered, however, by some of its drawbacks. Using UV wavelengths requires stringent precautions when compared to visible and NIR wavelengths: scattered UV can cause melanomas [92, 93] and cataracts [94, 95] in lab personnel. Goggles, long sleeves and UV-opaque gloves are sufficient to ensure protection against inadvertent exposure. Another consideration for using UV wavelengths is that special optical materials must be used to obtain the highest quality results. Fused silica and quartz with special anti-reflection coatings are typically used in this regime to provide the highest optical transmission, but they are more costly and not available in many configurations (e.g. lens focal lengths). Objective lenses that are specially designed for UV transmission tend to be significantly more expensive and sometimes even not as efficient at transmitting these wavelengths as standard visible-wavelength objective lenses. Along those same lines, we commissioned the fabrication of custom-made fused silica AODs for our UV scanner and the optical material had a direct bearing on the complexity of our optical layout. Because of the high speed-of-sound in fused silica, we required an $\sim$20 mm aperture to obtain an angular resolution $>$100 spots [96]. Since it is difficult to fabricate an AOD with a circular aperture this large (the sound field would not be flat across the aperture), the AODs were made with a rectangular aperture. The rectangular aperture subsequently required the use of cylindrical lenses which increased the complexity, cost and difficulty of alignment.

The design constraints of using UV light can be circumvented with proper optical layout, but some of the physiological implications cannot be dismissed. Because Rayleigh scattering increases with the inverse fourth power of the wavelength and photolysis is not restricted to the focal plane with single-photon absorption, we were restricted to using *only* dissociated neuron cultures. One possible consequence of this can be seen in the example traces of figure 3: the axial resolution is relatively poor (>7 μm) and the photolytically evoked EPSPs often exhibited much longer decay times than expected ($>$50 ms). We attribute these observations to significant out-of-plane photolysis of caged glutamate. A high-concentration bolus of glutamate is released in the focal volume that resulted in the rapid rise and decay. This desired effect is superimposed with a much longer time course of depolarization as the out-of-focus glutamate slowly spreads a lower concentration of glutamate (aided by diffusion and perfusion) over the whole neuron, activating glutamate receptors at many distributed locations.

A further disadvantage of neurons growing in cultures is the fact that they have been mechanically dissociated such that they no longer retain their natural synaptic connection and glial support structures. The culturing procedure destroys the natural hippocampal geometry (one of the brain regions we investigate) and the *de novo* synapse formation is likely to be aberrant. The fact that these synapses form in an anomalous manner could also contribute to the slower EPSP kinetics. We were able to confirm that the cultured neurons did, indeed, form new synapses by filling the neurons with a visible-excited structural dye and imaging on a standard epi-fluorescence microscope (data not shown). A further drawback was that we were not able to distinguish these atypical spines while performing a UV photolysis experiment. Three options are available to visualize the neurons. First, we might have patch-dialyzed the neurons with a UV-excitable fluorescent dye. Imaging the neurons at the same wavelength as photolysis is convenient because the imaging and photolysis systems are inherently registered and only one set of scan optics is required. This is the strategy we used in our multiphoton NIR scanner (section 6). In the case of our UV-based stimulator, we were reticent to use UV illumination for structural imaging because of the physical damage the neurons might incur from that wavelength range [97]. A second option would be to fill the neuron with a visible- or NIR-excited fluorescent dye, but this option would incur the expense of an additional scanning system (laser, AODs, optics) and the complexity of registering the two scan systems. A third option, the one we selected, involved straightforward bright-field trans-illumination with a standard filament lamp. This proved to be simple and cost effective, but strongly limited our ability to visually distinguish the low-contrast spines near the resolution limit of our objective lens.

We found that our NIR scanner (section 6) alleviated nearly all of the problems we encountered with the UV scanner. NIR wavelengths are much more convenient to manipulate: we were able to use optics constructed from standard materials (but with NIR anti-reflection coatings) and circular aperture AODs made from TeO_2. Despite the large disparity in the numbers of lenses and mirrors, construction and daily alignment of an all-spherical lens system is vastly more manageable than a cylindrical lens system. Because of the longer wavelength, Rayleigh scattering was much reduced, allowing the use of light-scattering preparations, such as acute brain slices. In addition, out-of-plane photolysis was negligible because of the small two-photon focal volume. Use of acute brain slices, in turn, largely preserved the natural circuitry, synaptic connections and support tissues found *in vivo*. In principle, the NIR scanner is quite capable of restricting glutamate photolysis in dissociated neuron cultures,

but we would have waived the advantages of using brain slices. The only significant category in which our NIR scanner underperforms our UV scanner is cost. The ultrafast Ti:S laser is by far more expensive, but the improvement in structural contrast, photolysis resolution, optical layout simplicity and physiological results far outweighs this cost.

We have shown that an AOD-controlled, fast-scanning, high-power laser beam focused to a diffraction-limited spot is a precise tool for generating complex, physiological synaptic activation patterns. Though the thrust of this paper has emphasized dendritic computation and synaptic summation because of our primary scientific interests, a multi-site photolytic stimulation instrument is useful for investigating many other neurophysiological facets. Such an instrument can be used to characterize synaptic dynamics [98], probe neural circuitry [45], map ligand-gated ion channels [99–101] and to investigate structural plasticity [102]. Beyond photolysis of caged neurotransmitters, a multi-site AOD-scanned laser microscope, when paired with a sensitive optical detector such as a photomultiplier tube, would extend its utility even further. A microscope of this sort would be particularly useful in functional imaging, such as tracking calcium and voltage dynamics in the thin dendritic branches [103, 104]. With precise, non-invasive experimental control over the inputs and outputs of a neuron, an investigator has a powerful tool with which to study a multitude of dendritic functions.

References

[1] Bugmann G 1997 Biologically plausible neural computation *Biosystems* **40** 11–9

[2] Euler T and Denk W 2001 Dendritic processing *Curr. Opin. Neurobiol.* **11** 415–22

[3] Häusser M and Mel B 2003 Dendrites: bug or feature? *Curr. Opin. Neurobiol.* **13** 372–83

[4] Mel B 1994 Information processing in dendritic trees *Neural Comput.* **6** 1031–85

[5] Mel B 1999 Why have dendrites? A computational perspective *Dendrites* (Oxford: Oxford University Press) pp 271–89

[6] Magee J 2000 Dendritic integration of excitatory synaptic input *Nature Rev.* **1** 181–90

[7] Koch C, Poggio T and Torre V 1983 Nonlinear interactions in a dendritic tree: localization, timing, and role in information processing *Proc. Natl Acad. Sci. USA* 80 2799–802

[8] Li X and Ascoli G 2006 Computational simulation of the input–output relationship in hippocampal pyramidal cells *J. Comput. Neurosci.* **21** 191–209

[9] Poirazi P, Brannon T and Mel B 2003 Arithmetic of subthreshold synaptic summation in a model CA1 pyramidal cell *Neuron* **37** 977–87

[10] Poirazi P, Brannon T and Mel B 2003 Pyramidal neuron as two-layer neural network *Neuron* **37** 989–99

[11] Polsky A, Mel B W and Schiller J 2004 Computational subunits in thin dendrites of pyramidal cells *Nat. Neurosci.* **7** 621–7

[12] Johnston D, Magee J, Colbert C and Christie B 1996 Active properties of neuronal dendrites *Ann. Rev. Neurosci.* **19** 165–86

[13] Callaway J and Ross W 1997 Spatial distribution of synaptically activated sodium concentration changes in cerebellar Purkinje neurons *J. Neurophysiol.* **77** 145–52

[14] Magee J and Johnston D 1995 Synaptic activation of voltage-gated channels in the dendrites of hippocampal pyramidal neurons *Science* **268** 301–4

[15] Magee J 1998 Dendritic hyperpolarization-activated currents modify the integrative properties of hippocampal CA1 pyramidal neurons *J. Neurosci.* **18** 7613–24

[16] Magee J 1999 Dendritic I_h normalizes temporal summation in hippocampal CA1 neurons *Nat. Neurosci.* **2** 508–14

[17] Fellous J-M, Rudolph M, Destexhe A and Sejnowski T 2003 Synaptic background noise controls the input/output characteristics of single cells in an *in vitro* model of *in vivo* activity *Neuroscience* **122** 811–29

[18] Dan Y and Poo M-M 2006 Spike timing-dependent plasticity: from synapse to perception *Physiol. Rev.* **86** 1033–48

[19] Mel B 1993 Synaptic integration in an excitable dendritic tree *J. Neurophysiol.* **70** 1086–101

[20] Margulis M and Tang C-M 1998 Temporal integration can readily switch between sublinear and supralinear summation *J. Neurophysiol.* **79** 2809–13

[21] Cash S and Yuste R 1998 Input summation by cultured pyramidal neurons is linear and position-independent *J. Neurosci.* **18** 10–5

[22] Cash S and Yuste R 1999 Linear summation of excitatory inputs by CA1 pyramidal neurons *Neuron* **2** 383–94

[23] Heck D, Borst A and Antkowiak B 2003 Passive spatial and temporal integration of excitatory synaptic inputs in cerebellar Purkinje cells of young rats *Neurosci. Lett.* **341** 79–83

[24] Liu G 2004 Local structural balance and functional interaction of excitatory and inhibitory synapses in hippocampal dendrites *Nature Neurosci.* **7** 373–9

[25] Gasparini S, Migliore M and Magee J 2004 On the initiation and propagation of dendritic spikes in CA1 pyramidal neurons *J. Neurosci.* **24** 11046–56

[26] Gasparini S and Magee J 2006 State-dependent dendritic computation in hippocampal CA1 pyramidal neurons *J. Neurosci.* **26** 2088–100

[27] Losonczy A, Makara J and Magee J 2008 Compartmentalized dendritic plasticity and input feature storage in neurons *Nature* **452** 436–41

[28] Guzowski J, Knierim J and Moser E 2004 Ensemble dynamics of hippocampal regions CA3 and CA1 *Neuron* **44** 581–4

[29] Archie K A and Mel B W 2000 A model for intradendritic computation of binocular disparity *Nat. Neurosci.* **3** 54–63

[30] Rall W 1964 Theoretical significance of dendritic trees for neuronal input-output relations *Neural Theory and Modeling* ed R F Reiss (Palo Alto, CA: Stanford University Press) pp 73–97

[31] Krichmar J, Nasutoa S, Scorcionia R, Washington S and Ascoli G 2002 Effects of dendritic morphology on CA3 pyramidal cell electrophysiology: a simulation study *Brain Res.* **941** 11–28

[32] Ramón y Cajal S 1892 El nuevo concepto de la histoligia de los centros nerviosos *Rev. Ciencias Méd. Barcelona*

[33] Ramón y Cajal S 1909 *Histology of the Nervous System of Man and Vertebrates* vol 2 (Oxford: Oxford University Press)

[34] Fiala J and Harris K 1999 Dendrite structure *Dendrites* (Oxford: Oxford University Press) pp 1–34

[35] Mainen Z and Sejnowski T 1996 Influence of dendritic structure on firing pattern in model neocortical neurons *Nature* **382** 363–6

[36] Schaefer A, Larkum M, Sakmann B and Roth A 2003 Coincidence detection in pyramidal neurons is tuned by their dendritic branching pattern *J. Neurophysiol.* **89** 3143–54

[37] Vetter P, Roth A and Häusser M 2001 Propagation of action potentials in dendrites depends on dendritic morphology *J. Neurophysiol.* **85** 926–37
[38] Veselovsky N S, Engert F and Lux H D 1996 Fast local superfusion technique *Pflügers Arch.* **432** 351–4
[39] Murnick J G, Dubé G, Krupa B and Liu G 2002 High-resolution iontophoresis for single-synapse stimulation *J. Neurosci. Methods* **116** 65–75
[40] Callaway E M and Yuste R 2002 Stimulating neurons with light *Curr. Opin. Neurobiol.* **12** 587–92
[41] Adams S R and Tsien R Y 1993 Controlling cell chemistry with caged compounds *Ann. Rev. Physiol.* **55** 755–84
[42] Brown E B, Shear J B, Adams S R, Tsien R Y and Webb W W 1999 Photolysis of caged calcium in femtoliter volumes using two-photon excitation *Biophys. J.* **76** 489–99
[43] Ramesh D, Wieboldt R, Niu L, Carpenter B K and Hess G P 1993 Photolysis of a protecting group for the carboxyl function of neurotransmitters within 3 microseconds and with product quantum yield of 0.2 *Proc. Natl Acad. Sci. USA* **90** 11074–8
[44] Wieboldt R, Gee K R, Niu Li, Ramesh D, Carpenter B K and Hess G P 1994 Photolabile precursors of glutamate: synthesis, photochemical properties, and activation of glutamate receptors on a microsecond time scale *Proc. Natl Acad. Sci. USA* **91** 8752–6
[45] Callaway E M and Katz L C 1993 Photostimulation using caged glutamate reveals functional circuitry in living brain slices *Proc. Natl Acad. Sci. USA* **90** 7661–5
[46] Nerbonne J M 1986 Design and application of photolabile intracellular probes *Optical Methods in Cell Physiology* (New York: Society of General Physiologists and Wiley) pp 417–45
[47] Denk W 1997 Pulsing mercury arc lamps for uncaging and fast imaging *J. Neurosci. Methods* **72** 39–42
[48] Rapp G and Güth K 1988 A low cost high intensity flash device for photolysis experiments *Pflügers Arch. European J. Physiol.* **411** 200–3
[49] Bernardinelli Y, Haeberli C and Chatton J-Y 2005 Flash photolysis using a light emitting diode: an efficient, compact, and affordable solution *Cell Calcium* **37** 565–72
[50] Kleinfeld D, Mitra P P, Helmchen F and Denk W 1998 Fluctuations and stimulus-induced changes in blood flow observed in individual capillaries in layers 2 through 4 of rat neocortex *Proc. Natl Acad. Sci. USA* 95 15741–6
[51] Diaspro A (ed) 2001 *Confocal and Two-Photon Microscopy: Foundations, Applications and Advances* (New York: Wiley)
[52] Göppert-Mayer M 1931 Über elementarakte mit zwei quantensprüngen *Ann. Phys. (Leipzig)* **9** 273–95
[53] Denk W, Strickler J H and Webb W W 1990 Two-photon laser scanning fluorescence microscopy *Science* **248** 73–6
[54] Zipfel W R, Williams M and Webb W W 2003 Nonlinear magic: multiphoton microscopy in the biosciences *Nat. Biotechnol.* **21** 1369–77
[55] Masters B R and So P T C (eds) 2008 *Handbook of Biomedical Nonlinear Optical Microscopy* (Oxford: Oxford University Press)
[56] Parpura V and Haydon P G 1999 UV photolysis using a micromanipulated optical fiber to deliver UV energy directly to the sample *J. Neurosci. Methods* **87** 25–34
[57] Diels J C and Rudolph W 1996 *Ultrashort Laser Pulse Phenomena* (San Diego, CA: Academic)
[58] Wilson T and Sheppard C 1984 *Theory and Practice of Optical Scanning Microscopy* (San Diego, CA: Academic)
[59] Nikolenko V, Poskanzer K and Yuste R 2007 Two-photon photostimulation and imaging of neural circuits *Nat. Methods* **4** 943–50
[60] Nikolenko V, Watson B O, Araya R, Woodruff A, Peterka D S and Yuste R 2008 SLM microscopy: scanless two-photon imaging and photostimulation with spatial light modulators *Front. Neural Circuits* **2** 1–14
[61] Golan L, Reutsky I, Farah N and Shoham S 2009 Design and characteristics of holographic neural photo-stimulation systems *J. Neural Eng.* **6** 066004
[62] Bullen A, Patel S S and Saggau P 1997 High-speed, random-access fluorescence microscopy: I. High-resolution optical recording with voltage-sensitive dyes and ion indicators *Biophys. J.* **73** 477–91
[63] Bullen A and Saggau P 1999 High-speed, random-access fluorescence microscopy: II. Fast quantitative measurements with voltage-sensitive dyes *Biophys. J.* **76** 2272–87
[64] Salomé R, Kremer Y, Dieudonné S, Léger J-F, Krichevsky O, Wyard C, Chatenay D and Bourdieu L 2006 Ultrafast random-access scanning in two-photon microscopy using acousto-optic deflectors *J. Neurosci. Methods* **154** 161–74
[65] Kun Bi, Zeng S, Xue S, Sun J, Xiaohua Lv, Derong Li and Luo Q 2006 Position of the prism in a dispersion-compensated acousto-optic deflector for multiphoton imaging *Appl. Opt.* **45** 8560–5
[66] Zeng S, Xiaohua Lv, Zhan C, Chen Wei R, Xiong W, Jacques S L and Luo Q 2006 Simultaneous compensation for spatial and temporal dispersion of acousto-optical deflectors for two-dimensional scanning with a single prism *Opt. Lett.* **31** 1091–3
[67] Gordon E I 1966 A review of acoustooptical deflection and modulation devices *Appl. Opt.* **5** 1629–39
[68] Xu J and Stroud R 1992 *Acousto-Optic Devices: Principles, Design, and Applications* (New York: Wiley)
[69] Iyer V, Losavio B E, Patel S S and Saggau P 2002 Ultraviolet acousto-optic laser scanner for fast, graded, multi-site photolysis of caged neurotransmitter to investigate dendritic integration *Proc. 2nd Joint Conf. Engineering in Medicine and Biology (EMBS) and the Biomedical Engineering Society (BMES) vol 3,* pp 2101–2
[70] Shoham S, O'Connor D H, Sarkisov D V and Wang S S-H 2005 Rapid neurotransmitter uncaging in spatially defined patterns *Nat. Methods* **2** 837–43
[71] Brewer G, Toricelli J, Evege E and Price P 1993 Optimized survival of hippocampal neurons in B27-supplemented neurobasal, a new serum-free medium combination *J. Neurosci. Res.* **35** 567–76
[72] Pettit D, Wang S, Gee K and Augustine G 1997 Chemical two-photon uncaging: a novel approach to mapping glutamate receptors *Neuron* **19** 465–71
[73] Losavio B E, Iyer V and Saggau P 2009 Two-photon microscope for multi-site micro-photolysis of caged neurotransmitters in acute brain slices *J. Biomed. Opt.* **14** 064033
[74] Iyer V, Losavio B E and Saggau P 2002 Dispersion compensation for acousto-optic scanning two-photon microscopy *Proc. SPIE* **4620** 281–92
[75] Iyer V, Losavio B E and Saggau P 2003 Compensation of spatial and temporal dispersion for acousto-optic multiphoton laser-scanning microscopy *J. Biomed. Opt.* **8** 460–71
[76] Fork R L, Martinez O E and Gordon J P 1984 Negative dispersion using pairs of prisms *Opt. Lett.* **9** 150–2
[77] Lechleiter J D, Lin D-T and Sieneart I 2002 Multi-photon laser scanning microscopy using an acoustic optical deflector *Biophys. J.* **83** 2292–9
[78] Li D, Zeng S, Xiaohua Lv, Liu J, Rui Du, Jiang R, Chen W R and Luo Q 2007 Dispersion characteristics of acousto-optic deflector for scanning Gaussian laser beam of femtosecond pulses *Opt. Express* **15** 4726–34
[79] Canepari M, Nelson L, Papageorgiou G, Corrie J E T and Ogden D 2001 Photochemical and pharmacological

evaluation of 7-nitroindolinyl-and 4-methoxy-7-nitroindolinyl-amino acids as novel, fast caged neurotransmitters *J. Neurosci. Methods* **112** 29–42
[80] Saitoe M, Koshimoto H, Hirano M, Suga T and Kidokoro Y 1998 Distribution of functional glutamate receptors in cultured embryonic Drosophila myotubes revealed using focal release of L-glutamate from caged compound by laser *J. Neurosci. Methods* **80** 163–70
[81] Frick A, Zieglgansberger W and Dodt H-U 2001 Glutamate receptors form hot spots on apical dendrites of neocortical pyramidal neurons *J. Neurophysiol.* **86** 1412–21
[82] Smith M, Ellis-Davies G and Magee J 2003 Mechanism of the distance-dependent scaling of Schaffer collateral synapses in rat CA1 pyramidal neurons *J. Physiol.* **548** 245–58
[83] Losavio B E, Reddy G D, Colbert C M, Kakadiaris I A and Saggau P 2006 Combining optical imaging and computational modeling to analyze structure and function of living neurons *Engineering in Medicine and Biology Society 2006 EMBS '06: 28th Annual Int. Conf. of the IEEE* p 668
[84] Losavio B E, Liang Y, Santamaría-Pang A, Kakadiaris I A, Colbert C M and Saggau P 2008 Live neuron morphology automatically reconstructed from multiphoton and confocal imaging data *J. Neurophysiol.* **100** 2422–9
[85] Rodriguez A, Ehlenberger D B, Dickstein D L, Hof P R and Wearne S L 2008 Automated three-dimensional detection and shape classification of dendritic spines from fluorescence microscopy images *PLoS ONE* **3(4)** e1997
[86] Fan J, Zhou X, Dy J G, Zhang Y and Wong S T C 2009 An automated pipeline for dendrite spine detection and tracking of 3D optical microscopy neuron images of *in vivo* mouse models *Neuroinformatics* **7** 113–30
[87] Rickgauer J P and Tank D W 2009 Two-photon excitation of channelrhodopsin-2 at saturation *Proc. Natl Acad. Sci* **106** 15025–30
[88] Mohanty S K, Reinscheid R K, Liu X, Okamura N, Krasieva T B and Berns M W 2008 In-depth activation of channelrhodopsin 2-sensitized excitable cells with high spatial resolution using two-photon excitation with a near-infrared laser microbeam *Biophys. J.* **95** 3916–26
[89] Banghart M, Borges K, Isacoff E, Trauner D and Kramer R 2004 Light-activated ion channels for remote control of neuronal firing *Nat. Neurosci.* **7** 1381–6
[90] Kramer R, Chambers J and Trauner D 2005 Photochemical tools for remote control of ion channels in excitable cells *Nature Chem. Biol.* **1** 360–5
[91] Kramer R H, Fortin D L and Trauner D 2009 New photochemical tools for controlling neuronal activity *Curr. Opin. Neurobiol.* **19** 544–52
[92] Wang S Q, Setlow R, Berwick M, Polsky D, Marghoob A A, Kopf A W, Robert S and Bart 2001 Ultraviolet A and melanoma: a review *J. Am. Acad. Dermatol.* **44** 837–46
[93] Gallagher R P and Lee T K 2006 Adverse effects of ultraviolet radiation: a brief review *Prog. Biophys. Mol. Biol.* **92** 119–31
[94] Javitt J C, Wang F and West S K 1996 Blindness due to cataract: epidemiology and prevention *Ann. Rev. Public Health* **17** 159–77
[95] Robman L and Taylor H 2005 External factors in the development of cataract *Eye* **19** 1074–82
[96] Gottlieb M, Ireland C and Ley J 1983 Acousto-optic interactions *Electro-optic and Acousto-Optic Scanning and Deflection* (New York: Dekker) pp 109–11
[97] Gentile M, Latonen L and Laiho M 2003 Cell cycle arrest and apoptosis provoked by UV radiation-induced DNA damage are transcriptionally highly divergent responses *Nucleic Acids Res.* **31** 4779–90
[98] Carnevale N T and Johnston D 1982 Electrophysiological characterization of remote chemical synapses *J. Neurophysiol.* **47** 606–21
[99] Denk W 1994 Two-photon scanning photochemical microscopy: mapping ligand-gated ion channel distributions *Proc. Natl Acad. Sci. USA* **91** 6629–33
[100] Pettit D L and Augustine G J 2000 Distribution of functional glutamate and GABA receptors on hippocampal pyramidal cells and interneurons *J. Neurophysiol.* **84** 28–38
[101] Lowe G 2003 Flash photolysis reveals a diversity of ionotropic glutamate receptors on the mitral cell somatodendritic membrane *J. Neurophysiol.* **90** 1737–46
[102] Matsuzaki M, Honkura N, Ellis-Davies G C R and Kasai H 2004 Structural basis of long-term potentiation in single dendritic spines *Nature* **429** 761–6
[103] Piston D W 1999 Imaging living cells and tissues by two-photon excitation microscopy *Trends Cell Biol.* **9** 66–9
[104] Iyer V, Hoogland T M and Saggau P 2006 Fast functional imaging of single neurons using random-access multiphoton (RAMP) microscopy *J. Neurophysiol.* **95** 535–45